

1 **A semi-automated technique for adenoma quantification in the**
2 ***Apc^{Min}* mouse using *FeatureCounter***

3 Amy L. Shepherd¹, A. Alexander T. Smith¹, Kirsty A. Wakelin¹, Sabine Kuhn¹, Jianping
4 Yang¹, David A. Eccles¹ and Franca Ronchese^{1*}

5

6 ¹Malaghan Institute of Medical Research, Wellington, New Zealand.

7

8

9

10 *To whom correspondence should be addressed at:

11 fronchese@malaghan.org.nz

12 Malaghan Institute of Medical Research

13 PO Box 7060

14 Newtown, Wellington 6242

15 New Zealand

16

17 **Keywords:** ImageJ, Automated tumour analysis, Intestinal tumours, *Apc^{Min}*, Tumour burden,

18 Linear Discriminant Analysis (LDA), Machine Learning

19

20

21 **ABSTRACT**

22 Colorectal cancer is a major contributor to death and disease worldwide. The *Apc^{Min}* mouse is
23 a widely used model of intestinal neoplasia, as it carries a mutation also found in human
24 colorectal cancers. However, the method most commonly used to quantify tumour burden in
25 these mice is manual adenoma counting, which is time consuming and poorly suited to
26 standardization across different laboratories. We describe a method to produce suitable
27 photographs of the small intestine, process them with an ImageJ macro, *FeatureCounter*,
28 which automatically locates image features potentially corresponding to adenomas, and a
29 machine learning pipeline to identify and quantify them. Compared to a manual method, the
30 specificity (or True Negative Rate, TNR) and sensitivity (or True Positive Rate, TPR) of this
31 method in detecting adenomas are similarly high at about 80% and 87%, respectively.
32 Importantly, total adenoma area measures derived from the automatically-called tumours were
33 just as capable of distinguishing high-burden from low-burden mice as those established
34 manually. Overall, our strategy is quicker, helps control experimenter bias and yields a greater
35 wealth of information about each tumour, thus providing a convenient route to getting
36 consistent and reliable results from a study.

37

38

39 INTRODUCTION

40 Human colorectal cancer is a major contributor to both disease and death in the Western
41 world, with approximately 1.36 million cases diagnosed in 2012 ¹. Due to the massive impact
42 of colorectal cancer worldwide, many animal models have been created to understand this
43 disease and test potential treatments. Mutations in the Wingless/Int-1 (Wnt) pathway are
44 commonplace in human colorectal cancer ². The Adenomatous polyposis coli (APC) protein is
45 part of the canonical Wnt pathway, which is strongly conserved across many species,
46 including humans and mice. APC promotes the destruction of β -catenin and prevents Wnt
47 signalling. Interestingly, the *Apc* gene is mutated in over 80% of colorectal cancer cases, as
48 well as in some breast cancers ³. One of the *Apc* mutations is particularly noteworthy, as it
49 causes Familial Adenomatous Polyposis ⁴. This hereditary genetic disease causes thousands of
50 polyps to form in the colon of the patient, which will invariably lead to colorectal cancer if
51 that patient is not screened and treated.

52 The *Apc^{Min}* mouse is a widely used model of spontaneously occurring intestinal tumours that
53 closely model human Familial Adenomatous Polyposis⁵. *Apc^{Min}* mice have been highly
54 valuable in demonstrating key mechanisms in colorectal cancer, for example, the importance
55 of Vascular Endothelial Growth Factor in the initial growth of intestinal tumours ⁶, the role of
56 COX-2 in adenoma formation ⁷, and the role of IL-33 in promoting tumorigenesis by
57 modifying the tumor immune environment ⁸. *Apc^{Min}* mice produce an inactive, truncated APC
58 protein due to a mutation leading to a premature stop codon in the *Apc* gene ⁹. This functional
59 loss in *Apc^{Min}* mice favours aberrant cell growth and, ultimately, spontaneous adenoma
60 generation in the mouse intestinal tract. Adenomas continue to grow throughout the mouse's
61 life, eventually causing bleeding, anaemia, and death, suggesting that tumour size, rather than

62 tumour count, may be a relevant metric.

63 Despite the wide use of the *Apc^{Min}* model, there is no standardized technique to quantify
64 adenoma burden in these mice. Most papers rely on complex protocols and report only on
65 manually-counted adenoma numbers, or numbers and areas in selected areas of the intestinal
66 tract, although some also include information on adenoma location and size. However, high
67 quality semi-automated methods are now becoming available to facilitate the identification of
68 tumour lesions in histological images¹⁰, or guide the visual classification of macroscopic
69 tumour lesions including melanomas in patients¹¹. Therefore, these methods can offer rapid
70 and objective tumour identification in a broad range of situations.

71 In this paper, we describe a protocol for preparing standardised, photography-based images of
72 mouse small intestine (SI), large intestine (LI) and caecum; a new ImageJ¹² software macro
73 called *FeatureCounter* that automatically identifies tumour-like features in the SI images and
74 extracts measures such as area; and a machine learning pipeline for classifying these features
75 as true adenomas or not. We illustrate this strategy's performance on 120 mice of different
76 genotypes, age and sex. On the whole, our approach extracts a more detailed picture of the
77 adenoma burden in mice in a standardized and reliable manner, enabling a rapid and more
78 sophisticated analysis of the experimental results.

79

80 **RESULTS**

81 **Adenoma enumeration approaches**

82 Unbiased and reliable evaluation of tumour burden is essential to the interpretation of the
83 results of any preclinical study addressing tumour biology and potential therapy. This is

84 normally achieved by blinding investigators to the treatment group and performing lengthy
85 manual quantification under a microscope. Nonetheless, individual variations in measurement
86 techniques make the standardization of results across different investigators difficult to
87 achieve. To overcome these limitations, we designed three new techniques to evaluate tumour
88 count and area in the SI of tumour-prone *Apc^{Min}* mice. The three techniques differed in degree
89 of automation, in how “features” of interest were identified, and in how those features were
90 classified or “called” as true Adenomas or not. A diagrammatic representation of the steps and
91 approximate time taken to perform a traditional method and these three new techniques are
92 shown in **Fig. 1**. A summary of these approaches is provided below:

- 93 1. The TRAD (Traditional) method involved dissecting the intestinal tract, longitudinally
94 opening the gut, spreading the tissue onto a petri dish or glass plate, and manually
95 enumerating tumours on fresh tissue using a stereomicroscope (**Supplementary Fig.**
96 **1**). The nature of these visually-identified tumours can be confirmed by standard
97 histological techniques as shown in **Supplementary Fig. 1**.
- 98 2. The DRAW approach involved dissecting the SI and removing all fat tissue, opening it
99 longitudinally taking care to leave any visible tumours intact, and carefully spreading
100 the tissue flat on a suitable cardboard as detailed in the Methods section. This was then
101 photographed close-up with a white ruler in shot for scale, and the photo stitched
102 together and opened using the Java-based image processing programme ImageJ ¹².
103 The image was scaled using the ruler, and the ImageJ ‘freehand selection’ function
104 was used to manually draw the margin of each of the visually-identified Ad. These
105 features were then measured and added up using the ImageJ’s ‘analyze particles’
106 function to generate adenoma numbers and area. The same approach was used also to

107 quantify tumours in the LI and caecum, after they were prepared similarly to the SI. In
108 this study, the DRAW approach identified no adenomas in the SI, caecum or LI from
109 control mice, indicating high researcher reliability when identifying tumours.

110 3. The CALL approach followed the DRAW approach up to the full SI image opening in
111 ImageJ. At this point, the *FeatureCounter* macro was run in ImageJ to automatically
112 set the scale and outline the contour of interesting features that might be adenomas.
113 From here, a researcher manually located each feature and “called” (assigned) them as
114 ‘true Adenomas’ (Ad) or ‘not Adenomas’ (nAd). The resulting information is used by
115 ImageJ ‘analyse particles’ function to calculate adenoma number and areas. Thus, the
116 CALL approach automatically identifies adenoma-like features that are then verified
117 by eye, providing a gold-standard training set for machine learning if required.

118 4. Finally, the LDA approach used the *FeatureCounter* macro-identified features
119 generated using the CALL approach and Linear Discriminant Aalysis (LDA, a
120 simple machine learning technique) to determine how to discriminate between Ad and
121 nAd features based on the feature measures. Once trained on a CALL dataset, this
122 method is fully automatic, and features can be delineated by *FeatureCounter* and then
123 classified as an Ad or nAd by the LDA.

124

125 **Photography and *FeatureCounter* can be faster than manual quantification**

126 We compared the time required to quantify SI tumours using the various approaches
127 described in **Fig. 1**. Preparing the SI for analysis using the TRAD approach took about 30
128 minutes. In contrast, the time to prepare and photograph one SI sample for all other
129 approaches took in total about 40 minutes, including sample dissection, washing,

130 photographing, and image stitching time. Similar quality images were obtained using either
131 fresh SI tissue or tissue that had been stored frozen and thawed before sample processing and
132 analysis. Use of frozen tissues added about 5-10 minutes to the total tissue preparation time,
133 but introduced a very useful experimental breakpoint option when immediate analysis was not
134 possible or highly inconvenient, as is often the case in survival studies.

135 The quantification of tumours using the TRAD approach, by visually quantifying tumours
136 under the dissecting microscope, took up to 60 minutes per sample depending on tumour
137 burden. Measurement of individual tumour sizes would add considerably to this time,
138 especially when the tumour burden is high. In the DRAW approach, tracing features by hand
139 in ImageJ took about 1 to 10 minutes per sample, again depending on tumour burden.

140 Running the *FeatureCounter* macro to automatically identify image features of interest took
141 about 15-30 seconds. Manually calling tumour features from the *FeatureCounter* macro's
142 features in the CALL approach took 1 to 5 minutes per sample, while the LDA approach
143 (assuming a streamlined processing pipeline) took only one minute to complete the analysis
144 across all 3188 features from 117 animals. It is immediately apparent that the main time gain
145 is in the ability to automatically identify and call features, which is highest on heavily tumour-
146 burdened mice. For low-burden mice, the extra preparation time would offset this gain;
147 however, the consistency and depth of data generated using the DRAW, CALL or LDA
148 methods may make the extra time investment beneficial compared to the TRAD approach.

149 Overall, the TRAD approach takes approximately 90 minutes per sample, the DRAW
150 approach 60 minutes, the CALL approach 50 minutes and the LDA method 45 minutes per
151 sample. **Figure 1** schematizes these four approaches along with time costs for each step of
152 each method.

153

154 **Tissue preparation and *FeatureCounter* True Positive Rate**

155 High quality tissue preparation is essential to tumour identification using the *FeatureCounter*
156 macro. **Figure 2A** shows a SI laid out on cardboard, before being bisected into two long
157 pieces which were then cut longitudinally and, using tweezers, opened out, spread flat with
158 smoothed edges, and cleaned with PBS to expose any adenomas present. A representative
159 image is presented in **Fig. 2B**. Tumours are visible as denser white areas on the blue
160 cardboard background. From these images, tumours were manually delineated by an
161 experienced researcher to generate the DRAW mask in **Fig. 2C**. Alternatively, the
162 *FeatureCounter* macro was used to automatically flag adenoma-like areas and generate a
163 mask as shown in **Fig. 2D**. *FeatureCounter* identified very few features from a good
164 preparation of control SI with no adenomas. Representative image and mask are shown in
165 **Fig. 2E** and **2F**, respectively. Common issues with tissue preparation and image analysis
166 include rolled edges, excess fat, patches of dried tissue, and light reflections which can all be
167 picked up as non-tumour features by the *FeatureCounter* macro (**Supplementary Fig. 2**).
168 These “false positive” image features can be largely avoided by first removing excess fat at
169 sample collection and then, during preparation, ensuring that the tissue edges are flat by
170 smoothing with tweezers, regularly moistening the samples once mounted, and finally
171 ensuring consistent camera and light placement during photography. Once the protocol is
172 learnt, it is relatively simple to avoid all these artifacts.

173

174 **Validation of tumour identification in the small intestine**

175 To ensure that our premise of identifying image features as actual adenomas was correct, we
176 carried out experiments where fresh SI tissue was spread on blue cardboard, analysed using
177 the DRAW method, and then used as a source of tissue for microscopic analysis. As shown in
178 **Fig. 3C and 3D**, two putative adenomas were selected due to their relatively isolated location
179 away from other tumours in the same sample, removed using a scalpel, then formalin fixed,
180 embedded in paraffin, and stained with haematoxylin and eosin. **Figure 3A and 3E** show a
181 magnification of these adenomas. Microscopic images in **Fig. 3B and 3F** revealed a typical
182 morphology with thickened mucosa, glandular appearance and a sessile structure. This
183 appearance is characteristic of adenomas as described in *Apc^{Min}* mice⁵ and very similar to that
184 of *Apc^{Min}* adenomas imaged in our Lab using standard methods such as Swiss rolling of
185 intestinal tissue (**Supplementary Fig. 1**).

186 As a further validation of the tumour-bearing status of *Apc^{Min}* mice as determined using the
187 DRAW method, we compared spleen and body weight between groups of *Apc^{Min}* mice and
188 their adenoma-free WT littermates, which were sacrificed at the same time or shortly after
189 euthanasia of the last surviving *Apc^{Min}* mouse in the same litter. A total of 49 mice, 27 *Apc^{Min}*
190 and 22 WT, were assessed. The average age of the *Apc^{Min}* mice was 149 days with SD of 37,
191 while the average age of the WT controls was 177 ± 21 days. The results in **Fig. 4** show that
192 spleen weight was significantly higher in *Apc^{Min}* mice compared to WT controls, while body
193 weight was lower. This is consistent with the reported anemia that develops in *Apc^{Min}* mice
194 with increasing tumour burden, which in turn leads to splenomegaly⁵. All *Apc^{Min}* mice
195 harboured numerous adenomas in the SI and a considerable tumour burden measured as total
196 tumour surface throughout the SI. No tumours were detected in the WT littermates.

197

198 **Linear Discriminant Analysis setup and feasibility**

199 We postulated that it would be possible to identify the true adenomas amongst the SI image
200 features delineated by *FeatureCounter* using data from the 22 shape and colour feature
201 measures provided by ImageJ. For example, one might expect adenomas to have rounder
202 shapes and slightly different colour than fat deposits and other non-tumour features. We thus
203 investigated the use of machine learning techniques for separating the true adenomas, “Ad”,
204 from not true adenomas, “nAd”. To provide a full training data for such a classifier, all the
205 image features from 120 mice with complete measures were called as Ad or nAd by a blinded,
206 experienced researcher using the CALL method. The dataset ultimately contained 3447 image
207 features (1286 Ad, 1919 nAd, rest unclassified).

208 As a first analysis, we performed a PCA of the of the image feature data generated using
209 *FeatureCounter*. It was quickly apparent that there was segregation – though imperfect –
210 between the Ad and nAd classes (**see Supplementary Fig. 3**), suggesting that it was likely
211 that the LDA would be able to identify true Ad from nAd. We thus pursued the LDA to try
212 and automatically separate the feature classes based on the measure data.

213 Non-independence of observations can be a major problem in any statistical methodology not
214 designed to take it into account, as is the case for LDA. Here, observations (image features)
215 are nested within mice, in other words, many features may be found in the same mouse,
216 potentially causing non-independence of observations. This may be an issue if, for example, a
217 generally low-quality gut preparation led to bias in one or more image feature measurements
218 across all features from that mouse: the LDA learning would include this bias and thus fail to
219 generalize properly to all features. We thus used the PCA in **Supplementary Fig. 3** to
220 highlight potential mouse-level biases. As shown in **Supplementary Fig. 3**, the barycentres of

221 most of the 120 mice clustered at the center of the PCA, indicating no major mouse-level bias.
222 For animals with barycentres not clustering within this central area, SI photographs were
223 retrieved and scrutinized for signs of substandard preparation. We concluded that 3 mice had
224 photography of insufficient quality due to either poor sample preparation or inappropriate
225 camera settings. After excluding these, no such bias was observed. This result emphasises the
226 importance of standardising the tissue preparation and photography protocols to minimise
227 sample batch effects. After this step, 3188 features with proper CALL classifications (1279
228 Ad (40.1%) and 1909 nAd (59.9%)) from 117 mice were retained for training the classifier.

229

230 **Linear Discriminant Analysis performance**

231 As with any classification strategy, it is good practice to perform a validation experiment to
232 assess the classifier's stability and performance when faced with novel data; in other words,
233 we wanted to check that the LDA classification strategy would perform well when applied to
234 real-world experimental numbers. Using a "bootstrapping" random sampling with
235 replacement strategy (see LDA validation in Methods), we generated a total of 4000
236 validation datasets, computationally representing the equivalent number of 'experiments' of
237 normal *Apc^{Min}* and WT animals, and each was used to train a separate LDA. We chose a
238 bootstrapping approach due to the relatively smaller size of our dataset, and selected with
239 replacement to ensure that population distribution was maintained for selections within each
240 validation dataset. For each validation set, feature-level performance indicators including
241 accuracy, TPR and Positive Predictive Value (PPV, or precision) and dataset-wide
242 performance indicators (such as the ratio of positive adenoma calls over true adenomas) were
243 derived for Ad and nAd on the full dataset, and compared to those obtained using LDA on the

244 full dataset, as described in the Methods.

245 The distributions of the feature-level performance indicators are presented in **Fig. 5A and 5B**.

246 The accuracy achieved for the full dataset was of 87%. The TPR (or the percent of the true Ad

247 / nAd correctly identified as such by the LDA) for the full LDA of Ad and nAd were close to

248 80% and 90%, respectively, indicating that the LDA was identifying correctly the majority of

249 both real Ad and nAd features. The PPV (or the proportion of the features identified as Ad /

250 nAd by the LDA that were correctly identified) of Ad or nAd were approximately 85% and

251 87% respectively, again showing good performance of the full LDA to classify Ad and nAd

252 features. Unsurprisingly, the LDA done on the whole dataset outperformed the majority of

253 bootstrapping datasets, perhaps indicating a slight overfitting when using the full dataset.

254 Nonetheless, all the indicators obtained on the validated datasets remained strong (indeed, the

255 worst performing indicator was Ad.TPR, with only 75% of values above 75%).

256 Importantly, the LDA performed very well when considering mouse-level performance

257 indicators. The Ad.ratio represents the ratio of the LDA-derived Ad count over the CALL-

258 provided Ad-count; the nAd.ratio is a similar indicator for nAd features. If the LDA was, in

259 practice, perfect, these ratios would be of exactly 1 (although it should be noted that the

260 converse is not true, and a ratio of 1 does not correspond to perfect performance). We

261 observed that the majority (the “most average 50%”, as indicated by the gray boxes in **Fig.**

262 **5B**) of validation dataset Ad.ratios were between 0.919 and 1.051, with a median of 0.984,

263 while the whole dataset achieved an Ad.ratio of 0.941. The nAd.ratio performed arguably

264 even better, with the majority of validation dataset nAd.ratios being between 0.965 and 1.054

265 with a median of 1.010, compared to an overall dataset performance of 1.04. Full indicator

266 quantiles are given in **Tables S3 & S4**, with the 0% and 100% quantiles indicating the

267 minimum and maximum values, that is, 0% and 100% of datasets below the indicated values,
268 respectively. Taken together, these results indicate that despite the presence of a low
269 frequency of inaccurate tumour callings, the estimated mouse-level tumour count is highly
270 accurate.

271 Both the adenoma numbers and the total adenoma areas calculated by LDA showed high
272 correlation to the values obtained using DRAW or CALL. Concordance between LDA and
273 CALL was very good, in general with LDA obtaining only slightly less Ad counts than
274 CALL, as shown by the regression line & confidence region thereof in **Fig. 5C**. Quite
275 interestingly, the total Ad area was a much more accurate and consistent mouse-level measure
276 compared to the number of Ad, as evidenced by the tight regression line in **Fig. 5E**.

277 Unsurprisingly, the LDA approach yields mouse-level measures closer to those of CALL
278 rather than that of DRAW, as it was trained and used on adenoma callings from the CALL
279 approach (**Fig. 5D for counts and 5F for area**); however, all three approaches generate
280 similar tumour number and total tumour area measures, indicating a good predictive value
281 across the three methods.

282

283 **Adenoma area is a valuable measure of tumour burden**

284 Many previous papers have used total tumour number as the only measurement of tumour
285 burden to assess the effects of various treatments on *Apc^{Min}* mice (for example, ¹³⁻¹⁵).

286 However, this does not take into account the size of the tumours, which can also be highly
287 variable.

288 The automated method described here greatly facilitates the measurement of total adenoma

289 area. We investigated how appropriate total adenoma area is as a measure of tumour burden.
290 **Figure 6A** illustrates why total area should be measured and recorded: it presents two
291 samples with identical tumour counts, but largely different tumour sizes. Biologically, larger
292 tumours in the colon have been shown to be associated with shorter patient survival, showing
293 the importance of considering tumour size as well as number in response to treatments ^{16,17}.
294 Furthermore, **Fig. 6B** illustrates that, in a sample of 63 mice evaluated using the DRAW
295 method, the average area of each tumour varied between different sections of the intestinal
296 tract, with tumours in the LI being significantly larger on average than SI tumours. We also
297 examined the correlation between total adenoma area and adenoma count in the SI. As shown
298 in **Fig. 6C**, the correlation between adenoma area and count was high, but the spread
299 increased with tumour number, thus reinforcing the utility of both measurements in evaluating
300 tumour status. Finally, we correlated the number and total area of tumours in the SI to spleen
301 weight, which represents a good surrogate measure of health status in *Apc^{Min}* mice. Total
302 tumour area in the SI was a better correlate of spleen weight than tumour number (**Fig. 6D**),
303 even when excluding a potential outlier ($R^2= 0.36$ vs. 0.43). We argue that these observations,
304 taken together, demonstrate the need to evaluate tumour area in addition to tumour count.

305

306 **Utility of the total adenoma area measurements as assessed by LDA**

307 To evaluate the usefulness and comparability of the tumour burden measures established by
308 the DRAW and LDA approaches, we compared their power to discriminate between tumour
309 burdens in mice of different ages (147 days or younger versus older than 147 days at the time
310 of sacrifice, which are expected to have different tumour burdens) as a proof of principle.
311 These comparisons are illustrated in **Fig. 7A-D**. Younger mice show a significantly lower

312 number of Ad and total Ad area than older mice, in both the DRAW and LDA method, thus
313 validating that both manual and automatic classification of SI features can distinguish
314 between lower numbers and area of adenomas. Unsurprisingly, differences were much more
315 pronounced for the area measures than the counts, further illustrating the utility of area as a
316 measure of tumour load.

317

318 **DISCUSSION**

319 We have developed a standardized protocol for first preparing and photographing mouse SI
320 samples, then for the manual (using the DRAW approach) or automatic (using an ImageJ
321 macro, *FeatureCounter*) identification of interesting image features (CALL approach), and
322 finally an LDA-based method for the automatic classification of said features as true
323 Adenomas or not Adenomas. Taken as a whole, these strategies allow for the consistent, rapid
324 and robust derivation of mouse-level tumour burden measures (both as adenoma count and
325 total adenoma area) for subsequent analysis.

326 Each of the steps in this standardized protocol works towards reducing technical, mouse-,
327 experimenter- and even institute-level bias and variability, thus increasing result
328 comparability and reproducibility. Additionally, the benefits are synergistic: as already
329 pointed out, more controlled sample preparation allows for more consistent feature
330 identification; and more consistently-defined features make feature classification easier. To
331 note, best results for training the LDA classifier would be expected by using training sets
332 called manually by either a single experimenter (as in this study), allowing the LDA to
333 “learn” the same cues as that experimenter, or by as many different experimenters as possible

334 (preferably across the same mice) allowing the LDA to “learn” the common cues to all.

335 Even with the best practice, however, the correct classification of image features by our LDA

336 step was not perfect. Most certainly, each step of our proposed method can be further

337 improved in future research. The use of diffuse lighting (such as a photography tent) at the

338 photography stage would minimise reflections that can be picked up as image features. The

339 *FeatureCounter* may be adjusted to detect less features in tumour-less images (for example,

340 by increasing the threshold size to ignore small features), while the automatic classification

341 may be adjusted or replaced with another machine learning methodology. For example, a

342 GLMNET algorithm ¹⁸ would allow the simultaneous selection and estimation of input

343 variable coefficients, at the very least leading to more consistent, if not more accurate, results.

344 More advanced machine learning algorithms, such as neural networks, are now being used in

345 the analysis of images from pathological samples, with new quantification approaches

346 becoming available (reviewed in ¹⁰). In some cases, deep neural networks have been shown to

347 deliver classifications that are as accurate as those of a specialist, as in the case of skin lesions

348 ¹¹. Therefore, neural networks, of which LDA is a simple, single node example, have the

349 potential to provide better classification of images such as those generated in this study. In

350 any case, manual verification by an experienced researcher can be rapidly and easily

351 associated with any of the protocols described here, and would be most conveniently carried

352 out after LDA corrects the most evident misclassifications, such as those resulting from

353 imperfect sample preparation or photography– although these are relatively rare once the

354 technique is learned (3/120 in this study).

355 Regardless, our semi-automated strategy is faster, more reliable and also more flexible than

356 previously used methods. Samples can be processed and analysed while fresh, or can be

357 frozen and analysed later at a convenient time. Through the sample freezing step, “break
358 points” are introduced into the experimental workflow, *i.e.* points at which the
359 experimentation for a single sample can be suspended temporarily, while in traditional
360 methods each sample is often prepared and counted the same day. The reduced time cost in
361 tumour quantification can be another major benefit in the DRAW, CALL and LDA
362 approaches. It is thus immediately apparent that, beyond the added flexibility, our automated
363 strategy may earn a considerable sample preparation and counting time gain when many mice
364 – especially heavily tumour-burdened ones – are being assessed. Furthermore, the preparation
365 techniques are accelerated further when processing multiple samples at a time. Additionally,
366 the wealth of data is higher using these approaches compared to the TRAD count method,
367 where just tumour number, or cumulative tumour area in a small section of the intestine, is
368 assessed. We also note that once digitized, the photographic information can be stored almost
369 indefinitely, allowing the data to be revisited if need be, for example, after a *FeatureCounter*
370 update, or after the implementation of a new classification methodology, or for meta-analysis.
371 Finally, if the effort of generating a large LDA training set was not justified, the CALL and
372 DRAW methods can be rapidly implemented, and are still quicker, more reliable, and
373 producing more detailed data than the traditional method.

374 Several previous papers (for example, ¹³⁻¹⁵) have only reported on total adenoma number,
375 using this as the lone tumour burden measure to assess the effects of various treatments on
376 *Apc^{Min}* mice. However, this does not take into account the size or aspect of the tumours, which
377 can be highly variable. For our part, we believe that adenoma count certainly cannot be used
378 alone, as area can differ for identical adenoma counts, and its distribution changes between
379 different segments of the mouse intestinal tract. The reasons for these similarities and

380 differences are multiple. For example, early studies of the *Apc^{Min}* mouse strain reported that
381 adenomas develop mostly during early life and up to puberty, and their numbers did not
382 increase after 100 days of age ¹⁹. After this stabilisation in numbers, the adenomas have been
383 observed to instead grow in size ²⁰, thus increasing tumour burden in a way not captured by
384 adenoma count alone. Additionally, significant size differences have been found in some
385 cases, demonstrating that area measures can provide additional information about treatments
386 or exacerbating conditions ²¹. For example, therapies may be effective at controlling adenoma
387 growth without fully eradicating tumours, an effect that would be detected as decreased
388 burden with little or no change in tumour number. We thus conclude that adenoma area, and
389 potentially other measures, are of sufficient importance and value to warrant the use of new
390 methods to facilitate collection of such information. As adenoma number is still generated
391 using our approach, comparisons to previous studies remain possible. Of note, with our
392 ImageJ feature-based approach, it is possible to derive several aggregate measures (for
393 example, average adenoma greyscale value per mouse, as listed in parameters in
394 **Supplementary Table 2**) that might relate back to tumour burden or other biological
395 indicators of interest. Further research in this direction may yield interesting insights.

396 In conclusion, we propose a semi-automated method to rapidly quantify tumour number and
397 associated tumour burden measures that will help alleviate biases, along with reproducibility
398 and consistency problems, which currently hamper efforts to interpret results across the
399 *Apc^{Min}* mouse literature. Our method is convenient, can be adapted to provide measurements
400 of several tumour characteristics, and will facilitate the use of *Apc^{Min}* mouse intestinal
401 adenoma model in a variety of applications.

402

403 **METHODS**

404 **Animals**

405 C57BL/6J-*Apc*^{Min} (*Apc*^{Min}) mice were purchased from The Jackson Laboratory (Bar Harbor,
406 ME) and bred in SPF conditions at the Malaghan Institute of Medical Research by mating
407 C57BL/6J-*Apc*^{Min/+} males with Wild-type (WT) C57BL/6J (*Apc*^{+/+}) females. *Apc*^{Min/+} and WT
408 offspring were identified by PCR and were both used in experimental conditions and pipeline
409 development. Water and standard laboratory chow were available *ad libitum*. All mice were
410 checked regularly for signs of anaemia and sickness, and were euthanized for tissue collection
411 if they developed pallor, low haematocrit (< 20%), weight loss, slow movement and/or
412 hunched posture.

413 All experimental protocols were approved by the Victoria University of Wellington Animal
414 Ethics Committee, and were carried out in accordance with the Victoria University of
415 Wellington Code of Ethical Conduct.

416

417 **Tissue preparation**

418 Mice were euthanized and the entire intestinal tract was extracted and sectioned into the SI,
419 caecum and LI. Special care was taken to remove as much mesenteric fat as possible. Sections
420 were washed thoroughly using PBS, drained, and analysed immediately or frozen in 6 well
421 plates at -80°C until further use.

422

423 **Photography**

424 For image analysis, SI tract sections were thawed (if frozen) and spread out in a thin
425 horseshoe shape on pieces of Steel Blue Germination paper (Anchor Paper Company, St
426 Pauls, MN, USA) approximately 25x10 cm in size. This colour was selected to enhance the
427 contrast between adenomas and the rest of the intestine. Once laid out on the paper, the SI was
428 cut into 2 equal pieces. Each piece was then cut longitudinally along the tube, opened and
429 edges spread flat using the edge of curved tweezers. Mucus and intestinal contents were
430 removed by spraying PBS on the tissue preparation, revealing any adenomas present. The
431 preparation was then photographed with a Panasonic Lumix G Vario DMX-G5W and a 45-
432 150 mm lens with additional 4x filter (Marumi, Japan), with a white ruler in shot. Multiple
433 pictures were taken and stitched together to reconstruct an image of the entire SI using the
434 software *Hugin* 2013.0.0²².

435 For the LI and caecum, a similar strategy was undertaken, where the tissue was placed on the
436 same type of Steel Blue Germination Paper as the SI, cut longitudinally (with multiple cuts
437 needed for the caecum), spread as flat as possible with special care taken to flatten tissue near
438 an adenoma in the caecum, and photographed with the white ruler in shot. Both the LI and the
439 caecum are small enough that they could be captured in one photograph.

440

441 **Manual delineation of tumours in images (DRAW approach)**

442 In order to enumerate and measure the area of tumours in the stitched images of SI, LI and
443 caecum, we used the Java-based image processing programme “ImageJ”
444 (<https://imagej.net>,¹²), which is freely available and able to analyse images in a variety of
445 formats. Full detail on tissue preparation, photography and analysis can be found at
446 https://gitlab.com/gringer/featurecounter/blob/master/Sample_Photography.pdf.

447 Images were scaled using a small macro and the white ruler in shot as a reference. ImageJ's
448 'freehand selection' function was then used to manually delineate visually-identified image
449 regions corresponding to adenomas. A scaled mask image was created using ImageJ's 'create
450 mask' function, and was analysed with the 'analyze particles' function to generate adenoma
451 numbers and measurements such as area. This is referred to as the "DRAW" approach.

452

453 ***FeatureCounter*, an ImageJ macro for the automatic identification of image features**

454 In order to automate the identification of image regions potentially corresponding to
455 adenomas from the photographs of intestinal sections as described in the DRAW approach,
456 we developed a more extensive ImageJ macro, called "*FeatureCounter*", focusing on SI
457 sections as these contain the large majority of the tumours that develop in *Apc^{Min}* mice. First,
458 *FeatureCounter* subtracts the blue background, leaving a grey scale image. It subsequently
459 performs automatic thresholding, before despeckling the image according to the parameters
460 listed in **Table S1**. This leaves areas of over 0.2mmsq in size, or "image features" that are
461 potentially tumours. The "analyse particles" function within ImageJ measures 22 variables for
462 each feature: Area, Perimeter, Mean, StdDev, Mode, Min, Max, Median, Skew, Kurt, Major,
463 Minor, Angle, Circularity, AR, Round, Solidity, Feret, FeretAngle, MinFeret, IntDen, and
464 RawIntDen. The details of these measures and their processing can be found in **Table S2**.
465 *FeatureCounter* was optimised to work on the SI due to its smooth and regular surface. It
466 does not perform as well at quantifying tumours in the LI, where the surface of the intestinal
467 wall is ridged, or in the caecum, where the tissue does not spread out flat particularly well. As
468 the number of tumours in the caecum and LI rarely exceeds 3 (mean and SD of LI and
469 caecum is 1.81 ± 2.00 and 0.41 ± 0.75 respectively), these tumours can be quickly and

470 accurately quantified manually from photos using the DRAW approach. Therefore, further
471 work to optimize *FeatureCounter* performance on the LI and caecum did not seem warranted,
472 and was not pursued.

473

474 **Manual validation of tumour features (CALL approach)**

475 Image features identified by *FeatureCounter* can be manually validated. After running
476 the macro, a user can manually assign or “call” which features are tumours, referring to
477 them as “Adenoma” (Ad) or “not-an-Adenoma” (nAd) or, for unclear features, ‘Not
478 Assigned’ (NA). In our study, there were relatively few NA features, and they were
479 consequently excluded from further analyses. We refer to this approach as the “CALL”
480 approach.

481 Of further interest, the image feature measures obtained from *FeatureCounter* can be
482 leveraged in a machine learning algorithm to automatically determine which features are
483 tumours and which are false positives. Such a machine learning algorithm would require
484 a gold-standard “training dataset”, i.e., a dataset of image features, their measurements,
485 and a prior validation of which features are indeed tumours or not, to learn tumour-
486 specific patterns. The CALL approach can be used to generate such a training set.

487

488 **Linear Discriminant Analysis (LDA) for automatic classification of image features**

489 Using the image feature measurements from *FeatureCounter* and a training dataset as
490 prepared using the CALL approach above, a machine learning technique can be used to
491 attempt to automatically separate tumour features from non-tumour features using the feature

492 measurements. LDA is one such supervised classification technique. It determines
493 discriminant functions – or the optimal linear combinations of the various input variables
494 (here: the 22 feature measures) – that can be used to classify statistical observations (here:
495 image features) into different classes (here: Ad or nAd). In our implementation, the *squares* of
496 the input variables were included as further input variables, as this allows quadratic
497 separations within the original variable space. All data were analysed within the R statistical
498 programming framework ²³.

499 LDA is sensitive to several influences, including 1) extreme non-normality in input variable
500 distributions and 2) extreme outliers in input variables. For these reasons, it is recommended
501 to pre-process the input variables. We manually examined the distributions of the feature
502 measure variables per class, and applied log10 transformations, shifted log10 transformations,
503 and imposed certain filters, as described in **Table S2**.

504 The applicability of LDA to the transformed feature data was first evaluated by performing a
505 Principal Components Analysis (PCA) with package *FactoMineR* ²⁴, the assumption being
506 that if the major axes of variability in the measurement data cannot segregate the classes even
507 partially, there is no point in performing an LDA and more advanced machine learning
508 techniques need to be used. The LDA was then performed using the *lda* function in the R
509 package *MASS* ²⁵ for features with no missing values. A link to the R script used to run the
510 LDA can be found in the Supplementary materials. We then proceeded to investigate the
511 performance of our LDA at two levels, described below: at the feature level (checking
512 whether the classification performed well) and at the mouse level (checking whether, in
513 practice, the methodology allowed for accurate tumour counting and area quantification).

514

515 **LDA feature-level and dataset-level performance**

516 We compared the LDA's feature-level predictions to the adenomas selected using the CALL
517 method, which were considered "true" adenomas in this instance. We considered as indicators
518 of the LDA's performance the True Positive Rate (TPR, or Sensitivity, here defined as the
519 proportion of all true Ad that were also identified as adenomas using LDA), the Positive
520 Predictive Value (PPV, or the proportion of the LDA-identified adenomas that were indeed
521 Ad), and the Accuracy (the proportion of all features correctly identified as Ad or nAd).
522 Similar calculations were done for the nAd classes.

523 As indicators of dataset-level performance of the CALL and LDA adenoma callings, we
524 counted the number of Ad and nAd calls, and calculated the ratios of the number of LDA-
525 predicted Ad and nAd over the number of CALL-provided Ad and nAd (Ad.ratio and
526 nAd.ratio, respectively). An LDA with perfect performance would generate ratios of exactly
527 1, although a value of 1 is not necessarily indicative of perfect performance.

528

529 **LDA validation**

530 To assess the robustness of the LDA's results, we performed a large validation experiment
531 with a complex re-sampling scheme inspired by those of mixed modelling/multi-level models.
532 We chose to randomly sample mice (with replacements, *i.e.* a same mouse can be sampled
533 more than once) from the 117 with appropriate data, including all their image features in each
534 validation dataset. Mice continued to be sampled until a) at least 12 mice (about 10.3% of the
535 total) had been sampled, and until b) at least 750 features (23.5% of total) had been sampled.
536 Indeed, as the choice of the feature number parameter in the re-sampling scheme strongly

537 influences the performance indicators, we empirically determined that a minimal feature
538 count of 750 presented the best trade-off between sample size and indicator performance
539 (**Supplementary Fig. 4**). Additionally, to ensure some measure of class balance, only datasets
540 with a composition containing at least 30% Ad features and 30% nAd features were retained.
541 A total of 4000 validation datasets were generated (computationally representing the
542 equivalent number of ‘experiments’ of normal *Apc^{Min}* and WT animals), and each was used to
543 train a separate LDA. For each validation LDA model, feature-level performance indicators
544 (Accuracy, TPR, PPV) and dataset-level performance indicators (Ad.ratio and nAd.ratio)
545 described above were derived using the whole dataset. For all indicators, we established their
546 quantiles of interest (0, 5, 25, 50, 75, 95, 100%) to compare to the values obtained on the full
547 dataset LDA.

548

549 **Statistics used to compare mouse-level results**

550 Comparisons of mouse data (weight, tumor numbers etc) used the Mann-Whitney U test or a
551 Kruskal-Wallis test followed by Dunn’s multiple comparison test, and were performed using
552 Prism 8.0 GraphPad software.

553 To compare adenoma results at the mouse level (counts, total areas) obtained using different
554 methods (CALL and LDA), we used Deming regression, a statistical technique used for
555 comparing two measurement methods for a same quantity, where *both* measurements are
556 assumed to have measurement error (typical linear regression only assumes error in the
557 outcome variable). We used the *mcreg* function implemented in package *mcr*²⁶ assuming a
558 variance ratio of 1, and using bootstrapping (n=999, ‘Bias-corrected and accelerated’ method)
559 to obtain a regression curve confidence area.

560

561 **Availability of Data and Materials**

562 The *FeatureCounter* ImageJ macro is freely available to download from

563 <https://gitlab.com/gringer/featurecounter/> together with instructions for photography, and

564 macro installation, some examples of tumour images, and the R code for running the

565 LDA. The datasets generated during the current study are available from the

566 corresponding author on reasonable request. Tumour images are available from Zenodo

567 repository. doi:10.5281/zenodo.3365777.

568

569

570 **REFERENCES**

- 571 1 GLOBOCAN. *Estimated cancer incidence, mortality and prevalence worldwide*
572 *in 2012, 2012*).
- 573 2 Half, E., Bercovich, D. & Rozen, P. Familial adenomatous polyposis. *Orphanet J*
574 *Rare Dis* **4**, 22, doi:10.1186/1750-1172-4-22 (2009).
- 575 3 Kinzler, K. W. & Vogelstein, B. Lessons from hereditary colorectal cancer. *Cell*
576 **87**, 159-170 (1996).
- 577 4 Nishisho, I. *et al.* Mutations of chromosome 5q21 genes in FAP and colorectal
578 cancer patients. *Science* **253**, 665-669 (1991).
- 579 5 Moser, A. R., Pitot, H. C. & Dove, W. F. A dominant mutation that predisposes
580 to multiple intestinal neoplasia in the mouse. *Science* **247**, 322-324 (1990).
- 581 6 Korsisaari, N. *et al.* Inhibition of VEGF-A prevents the angiogenic switch and
582 results in increased survival of Apc^{+/min} mice. *Proc Natl Acad Sci U S A* **104**,
583 10625-10630, doi:10.1073/pnas.0704213104 (2007).
- 584 7 Zhang, M. Z. *et al.* Inhibition of 11beta-hydroxysteroid dehydrogenase type II
585 selectively blocks the tumor COX-2 pathway and suppresses colon
586 carcinogenesis in mice and humans. *J Clin Invest* **119**, 876-885,
587 doi:10.1172/JCI37398 (2009).
- 588 8 He, Z. *et al.* Epithelial-derived IL-33 promotes intestinal tumorigenesis in Apc
589 (Min/+) mice. *Sci Rep* **7**, 5520, doi:10.1038/s41598-017-05716-z (2017).
- 590 9 Su, L. K. *et al.* Multiple intestinal neoplasia caused by a mutation in the
591 murine homolog of the APC gene. *Science* **256**, 668-670 (1992).

- 592 10 Wang, S., Yang, D. M., Rong, R., Zhan, X. & Xiao, G. Pathology Image Analysis
593 Using Segmentation Deep Learning Algorithms. *Am J Pathol*,
594 doi:10.1016/j.ajpath.2019.05.007 (2019).
- 595 11 Esteva, A. *et al.* Dermatologist-level classification of skin cancer with deep
596 neural networks. *Nature* **542**, 115-118, doi:10.1038/nature21056 (2017).
- 597 12 Schneider, C. A., Rasband, W. S. & Eliceiri, K. W. NIH Image to ImageJ: 25 years
598 of image analysis. *Nat Methods* **9**, 671-675 (2012).
- 599 13 Amos-Landgraf, J. M. *et al.* Sex disparity in colonic adenomagenesis involves
600 promotion by male hormones, not protection by female hormones. *Proc Natl*
601 *Acad Sci U S A* **111**, 16514-16519, doi:10.1073/pnas.1323064111 (2014).
- 602 14 Chae, W. J. & Bothwell, A. L. IL-17F deficiency inhibits small intestinal
603 tumorigenesis in ApcMin/+ mice. *Biochem Biophys Res Commun* **414**, 31-36,
604 doi:10.1016/j.bbrc.2011.09.016 (2011).
- 605 15 Maywald, R. L. *et al.* IL-33 activates tumor stroma to promote intestinal
606 polyposis. *Proc Natl Acad Sci U S A* **112**, E2487-2496,
607 doi:10.1073/pnas.1422445112 (2015).
- 608 16 Kornprat, P. *et al.* Value of tumor size as a prognostic variable in colorectal
609 cancer: a critical reappraisal. *Am J Clin Oncol* **34**, 43-49,
610 doi:10.1097/COC.0b013e3181cae8dd (2011).
- 611 17 Suzuki, C. *et al.* The initial change in tumor size predicts response and
612 survival in patients with metastatic colorectal cancer treated with
613 combination chemotherapy. *Ann Oncol* **23**, 948-954,
614 doi:10.1093/annonc/mdr350 (2012).

- 615 18 Friedman, J., Hastie, T. & Tibshirani, R. Regularization Paths for Generalized
616 Linear Models via Coordinate Descent. *J Stat Softw* **33**, 1-22 (2010).
- 617 19 Moser, A. R., Dove, W. F., Roth, K. A. & Gordon, J. I. The Min (multiple
618 intestinal neoplasia) mutation: its effect on gut epithelial cell differentiation
619 and interaction with a modifier system. *J Cell Biol* **116**, 1517-1526 (1992).
- 620 20 Kettunen, H. L., Kettunen, A. S. & Rautonen, N. E. Intestinal immune responses
621 in wild-type and *Apcmin/+* mouse, a model for colon cancer. *Cancer Res* **63**,
622 5136-5142 (2003).
- 623 21 McAlpine, C. A., Barak, Y., Matisse, I. & Cormier, R. T. Intestinal-specific
624 PPARgamma deficiency enhances tumorigenesis in *ApcMin/+* mice. *Int J*
625 *Cancer* **119**, 2339-2346, doi:10.1002/ijc.22115 (2006).
- 626 22 Desile, M. *Hugin 2013.0.0*, 2013).
- 627 23 Team, R. C. *R: A language and environment for statistical computing.*, 2013).
- 628 24 Husson, F., Josse, J., Le, S. & Mazet, J. *FactoMineR: Multivariate Exploratory*
629 *Data Analysis and Data Mining with R.* [http://CRAN.R-](http://CRAN.R-project.org/package=FactoMineR)
630 [project.org/package=FactoMineR](http://CRAN.R-project.org/package=FactoMineR), 2013).
- 631 25 Venables, W. N. & Ripley, B. D. *Modern Applied Statistics with S. Fourth*
632 *Edition.* . (Springer, 2002).
- 633 26 Manuilova, E., Schuetzenmeister, A. & Model, F. *MCR: method comparison*
634 *regression.* <http://CRAN.R-project.org/package=mcr>, 2014).
- 635
- 636
- 637

638 **Acknowledgements**

639 We sincerely thank all staff at the Malaghan Institute of Medical Research Biomedical
640 Research Unit for maintenance of the *Apc^{Min}* mouse strain. We thank Professor Terry Speed,
641 (Walter and Eliza Hall Institute of Medical Research) for helpful discussions about statistical
642 analysis. We also thank the Free and Open Source Software community for access to a
643 number of programs used over the course of this project. This work was funded by the A.M.
644 Duncan Bequest to the Malaghan Institute of Medical Research, and funding from the NZ
645 Cancer Society and the Health Research Council of NZ to FR.

646

647 **Author Contributions**

648 ALS developed and performed gut preparations, counted adenomas manually and classified
649 the automatically identified features, and wrote the manuscript. AATS carried out statistical
650 analyses of image features. KAW carried out adenoma validation and generated adenoma
651 data. SK and JY carried out TRAD quantifications. DAE developed the *FeatureCounter*
652 macro. FR supervised the project, provided support and suggestions for investigations, and
653 edited the manuscript. All authors provided suggestions and approved the final manuscript.

654

655 **Competing interests**

656 The authors declare no competing interests.

657

658

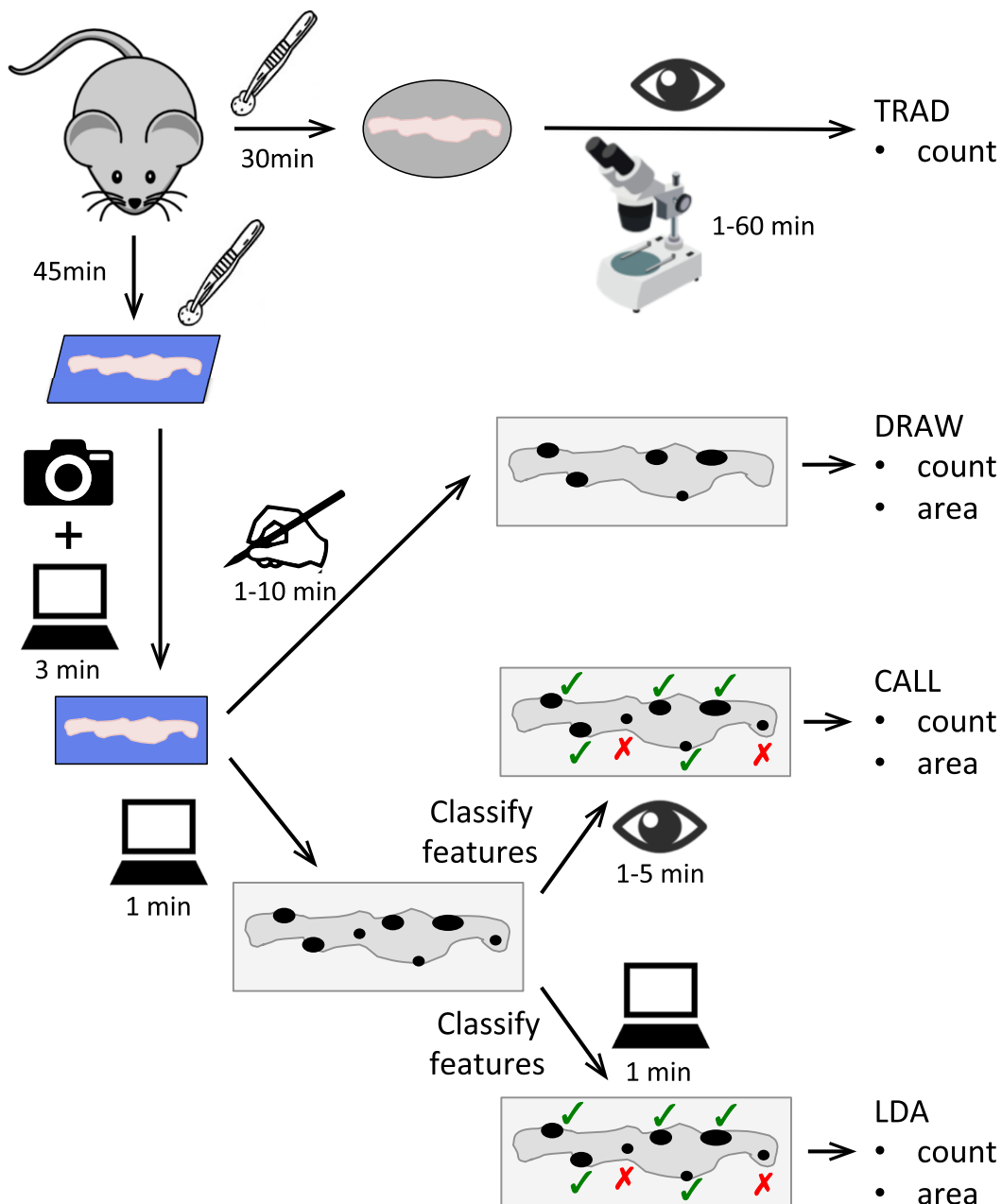


Figure 1. Schematic of the tumour measurement methods described in this paper.

Flow chart illustrating each step needed to perform the TRAD, DRAW, CALL, and LDA intestinal adenoma identification methods described in this paper. The icons represent the tools required to perform each step; estimated time costs per step are indicated. Please refer to the Materials & Methods and Results for a detailed description of the workflow for each method.

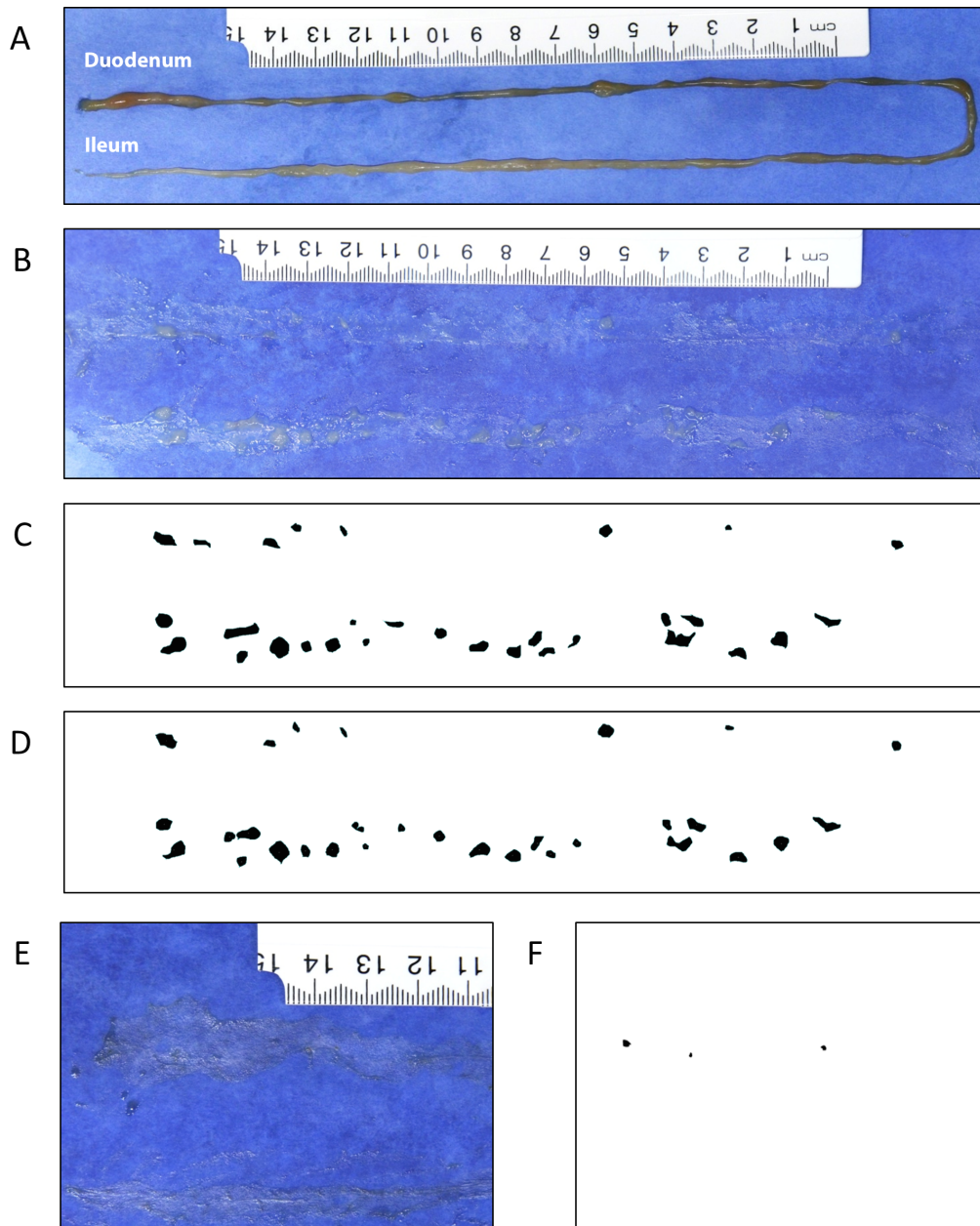


Figure 2. The image features (adenomas) identified by the automated *FeatureCounter* macro mostly correspond to adenomas as identified using the manual DRAW method

(A) Freshly collected SI from an *Apc^{Min}* mouse placed on blue cardboard. (B) The same SI after being cut longitudinally, spread and cleaned with PBS to expose tumours. (C) *FeatureCounter*-generated tumour mask for the same sample. (D) Manually-generated tumour mask for the same sample. (E) A representative partial picture of a control SI. (F) *FeatureCounter*-generated mask, showing features picked up on the section shown in E. No additional features were picked up from the complete image.

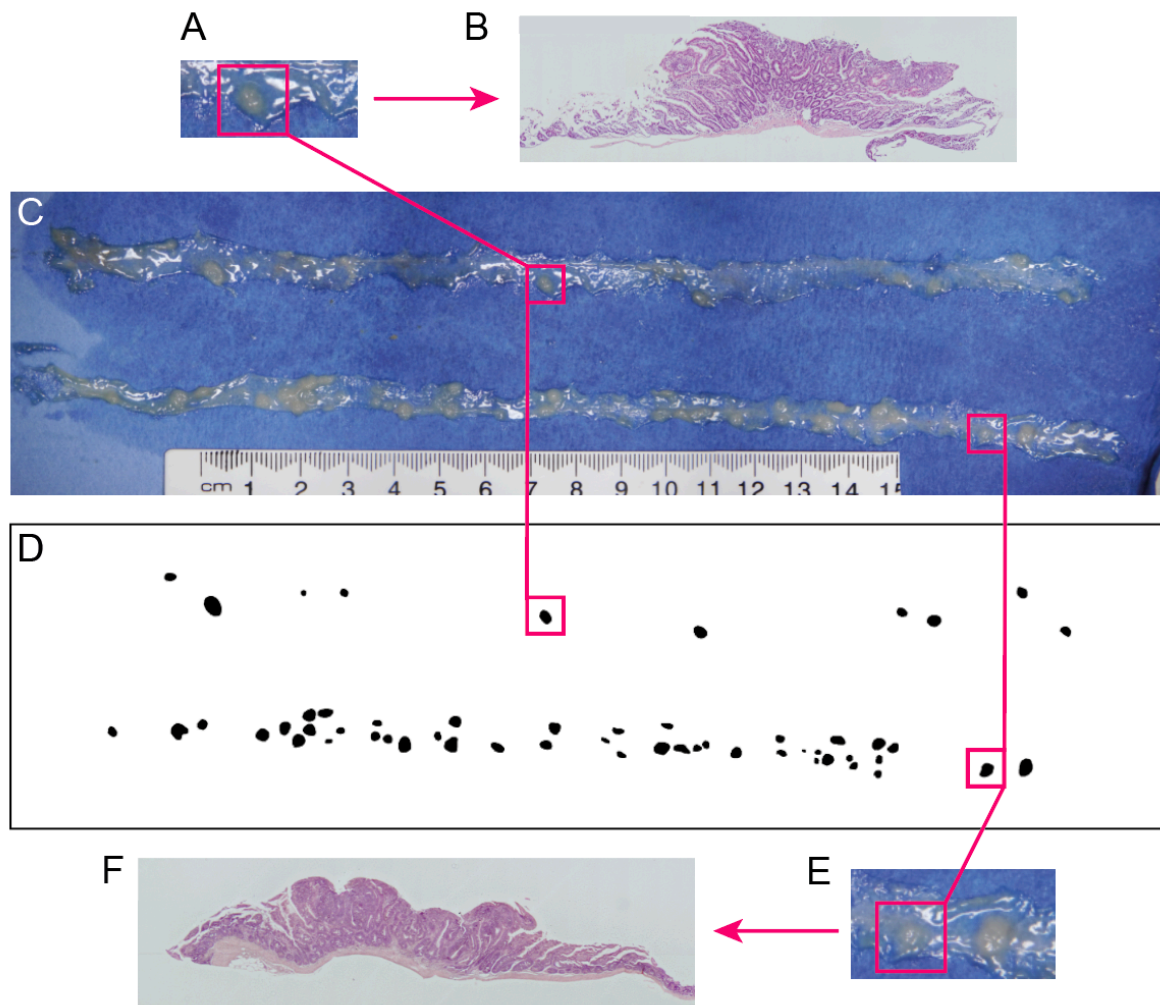


Figure 3. The image features identified using the DRAW method are adenomas.

Fresh SI tissue was isolated from *Apc^{Min}* mice, immediately set up on blue paper (C) and examined using the DRAW method in *FeatureCounter* to generate the mask in (D). Two relatively isolated features were chosen (marked by orange lines and magnified in B, E) excised from the paper support using a scalpel, and processed by formalin fixation, paraffin embedding and H&E staining to generate the images in (A) and (F). Data are from one of 3 mice and 7 SI tumours that were similarly treated and analysed.

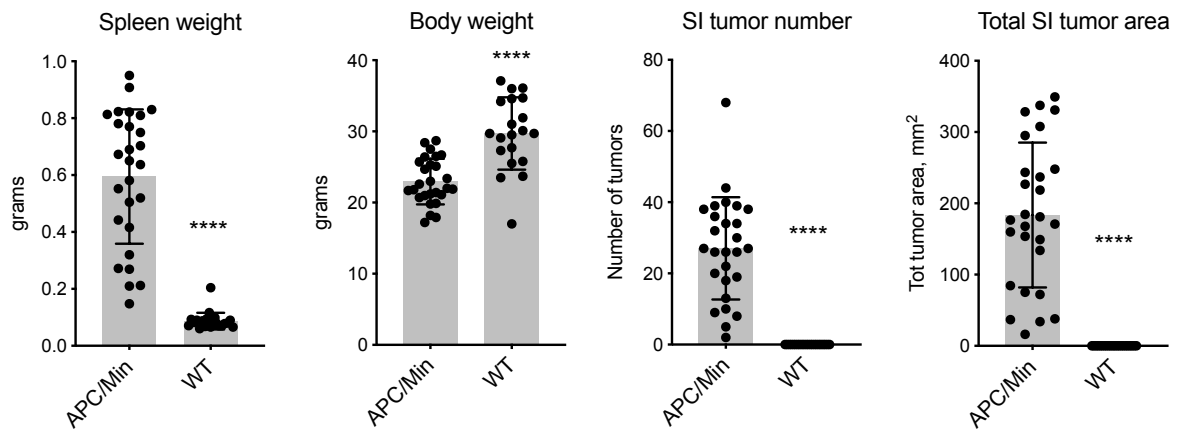


Figure 4. Spleen weight, body weight, number of SI tumors and their total area differ significantly between *Apc^{Min}* mice and their WT littermates.

Apc^{Min} mice (n=27, 13 females and 14 males) were sacrificed when anemic and their body and spleen weights were determined. SI tumor numbers and total area were determined as shown in Figure 2 using the DRAW method. WT littermates (n=22, 9 females and 13 males) were sacrificed together with, or soon after, the last surviving *Apc^{Min}* littermate. Average ages \pm SD were 149 ± 36 days for *Apc^{Min}* mice, and 177 ± 21 days for WT controls. Bar graphs show mean \pm SD, each dot represents one mouse. P values were calculated using a Mann-Whitney test, ****: $p < 0.0001$.

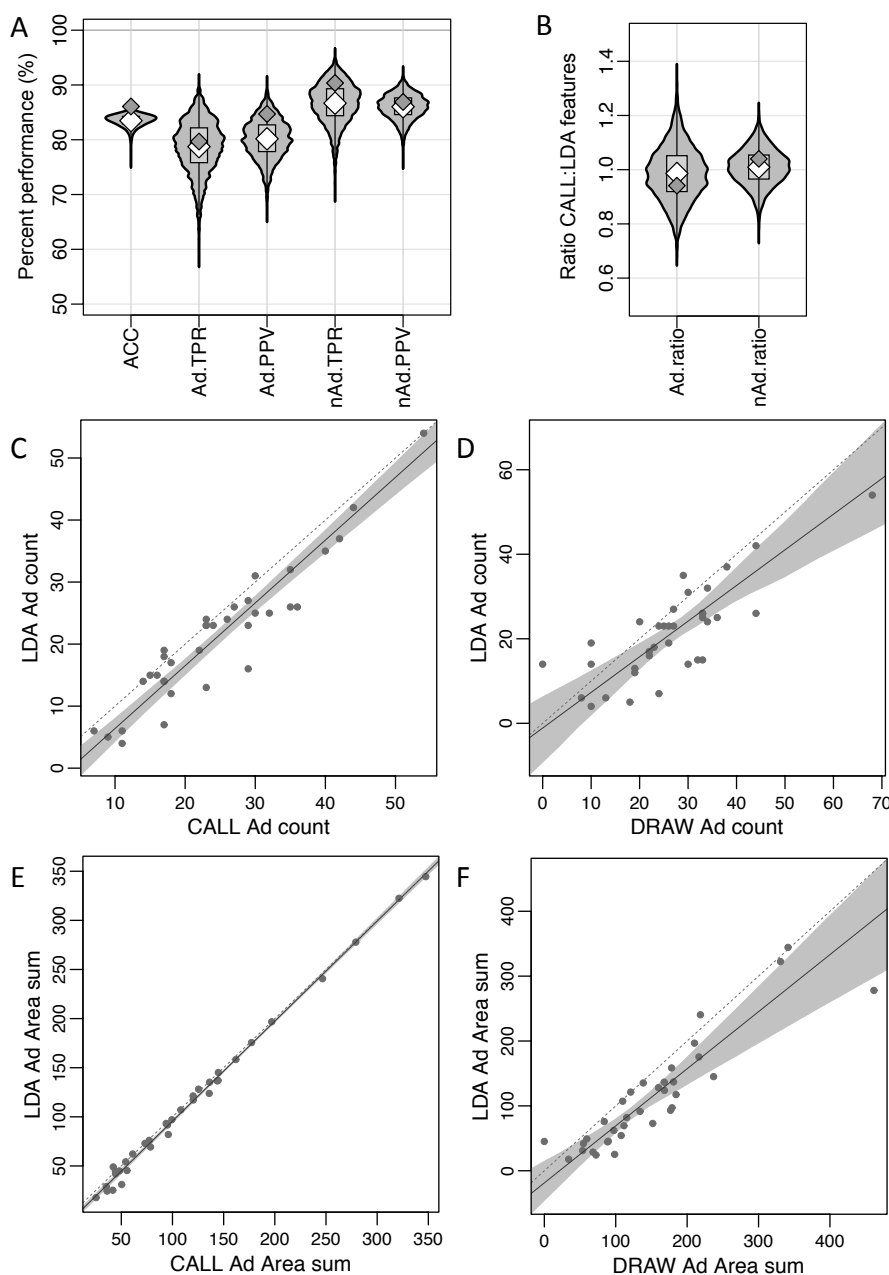


Figure 5. LDA predicts *Apc^{Min}* tumour count and area with similar accuracy to the CALL and DRAW approaches.

(A, B) Violin plots illustrating the distribution of the selected LDA performance indicators across the 4000 cross-validation datasets from 117 mice, each including 750-959 image features, when compared to the CALL-defined adenomas. The light grey violins are representative of the distribution of values obtained across the CV datasets; central grey boxes indicate the middle 50% of values; white diamonds represent median values for the CV datasets; dark grey diamonds represent the values observed in the full LDA. (A) shows Accuracy (ACC); Ad True Positive Rate (TPR, or sensitivity); Ad Positive Predictive Value (PPV); nAd TPR (or specificity); and nAd PPV distributions.

(B) The Ad.ratio is the ratio between the number of CALL Ad and LDA Ad, with a value of 1 indicating a perfect match. The nAd.ratio is determined similarly for nAd features.

(C-F) Deming regression plots comparing mouse-level adenoma number and total area values obtained through different approaches, for 35 mice. **(C)** compares adenoma counts generated by the LDA and CALL methods, **(D)** compares adenoma counts generated by the LDA and DRAW methods, **(E)** compares total adenoma area generated by the LDA and CALL methods, and **(F)** compares total adenoma area generated by the LDA and DRAW methods. Each dot corresponds to one mouse. Dotted grey line represents equality between measures. Solid grey line represents the regression line. Shaded grey area represents 95% confidence interval around the regression line.

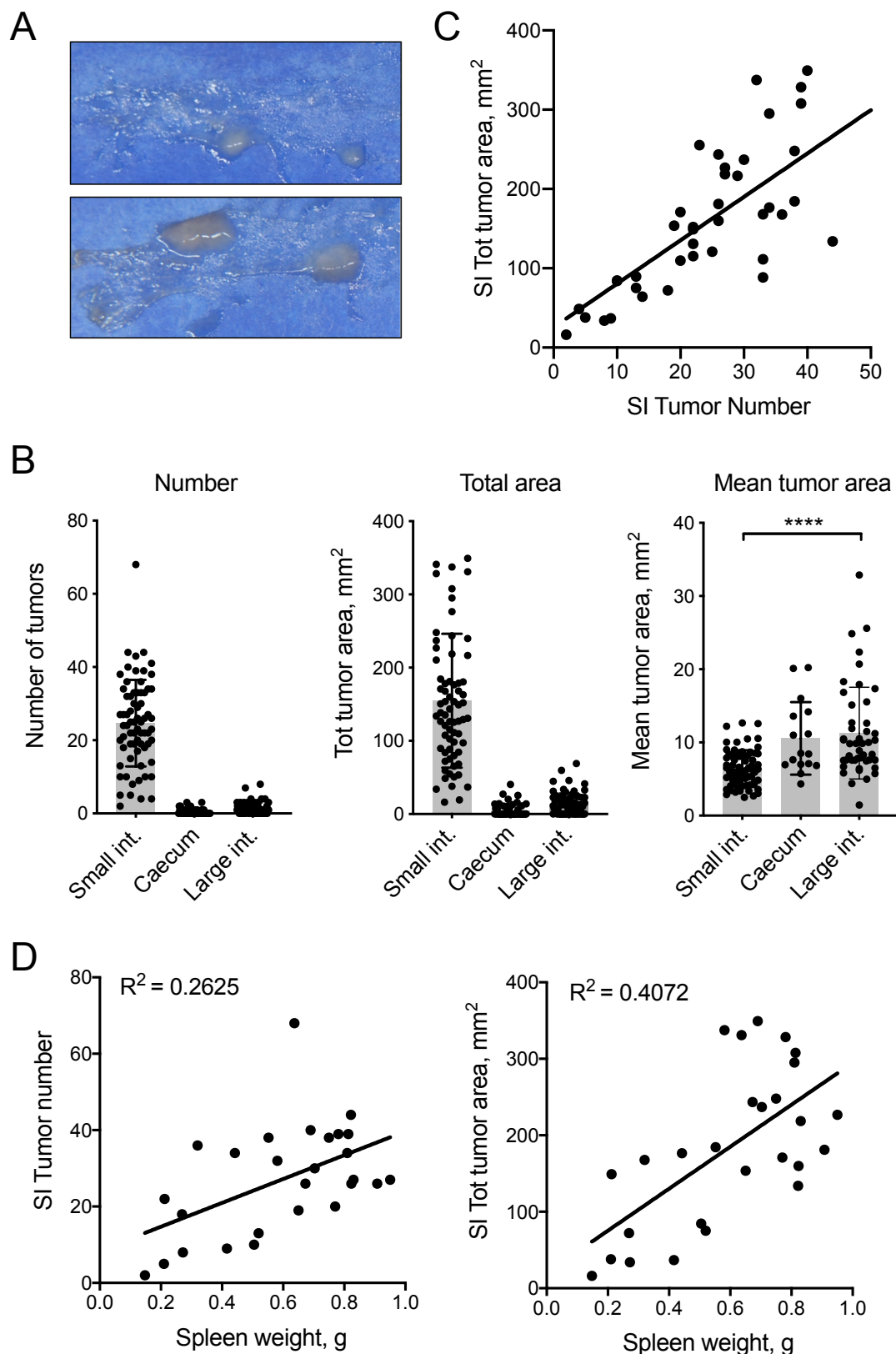


Figure 6. Total tumor area is an informative measure of tumour burden in *Apc*^{Min} mice.

(A) Duodenal samples from two *Apc*^{Min} mice, each with two tumours. Note the large difference in

tumour sizes between the two samples. **(B)** Bar graphs show the mean Number, Total area and Mean tumor area of tumours in different locations of the intestinal tract, +/- SD. Tumors were identified and measured using the DRAW method in a sample of 70 Apc^{Min} mice. Each dot represents a single mouse. ****: $p < 0.0001$ as determined using a Kruskal-Wallis test with Dunn's multiple comparison test. **(C)** Correlation between tumour count and size in LDA-called features in the SI of 35 mice. The dotted line represents the regression line. **(D)** Linear regression analysis of spleen weight vs. SI tumor number (left panel) or total area (right panel) in the SI of 27 mice for which spleen weight was available. Each dot represents one mouse. Data are from Figure 4.

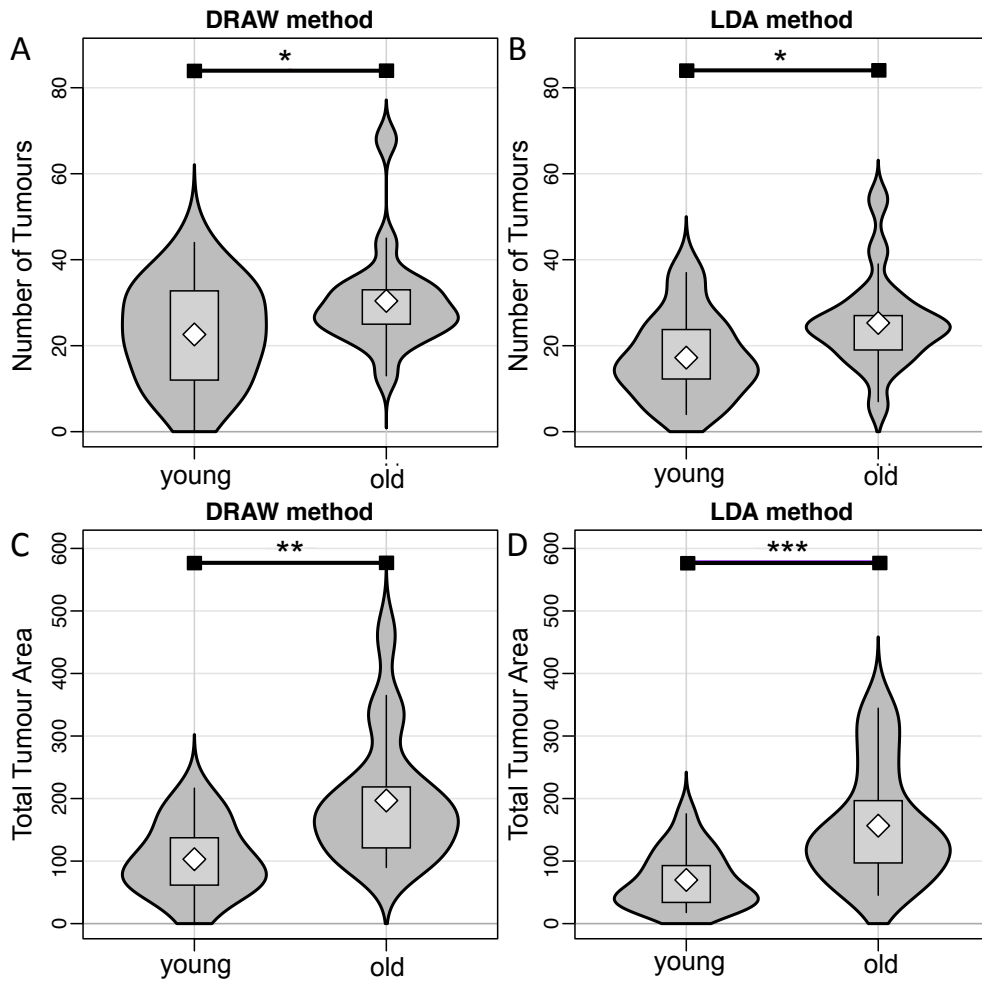


Figure 7. The DRAW and LDA methods both differentiate tumour number and total tumour area in young vs. old mice.

35 *Apc^{Min}* mice were sacrificed when anaemic and then split by age: ‘Young’ (n=18) range from 1-147 days, while ‘Old’ (n=17) range from 147-214 days. (A, B): Violin plots of the number of tumours enumerated by the DRAW method (A) and the LDA method (B). (C, D): Violin plots of total area of tumours calculated by the DRAW method (C) and the LDA method (D). Stars indicate significance at the 5% level for approximate one-tailed Mann-Whitney-Wilcoxon tests (*: $p < 0.05$, **: $p < 0.01$, ***= $p < 0.001$).